# Real-time organic aerosol characterization via Orbitrap mass spectrometry in urban and agricultural environments

5     Julia David[1], Luca D'Angelo[1], Mario Simon[1], Alexander L. Vogel[1]

[1] Institute for Atmospheric and Environmental Sciences, Goethe University Frankfurt, 60438 Frankfurt am Main, Germany

*Correspondence to*: Julia David (david@iau.uni-frankfurt.de), Alexander Lucas Vogel (vogel@iau.uni-frankfurt.de)
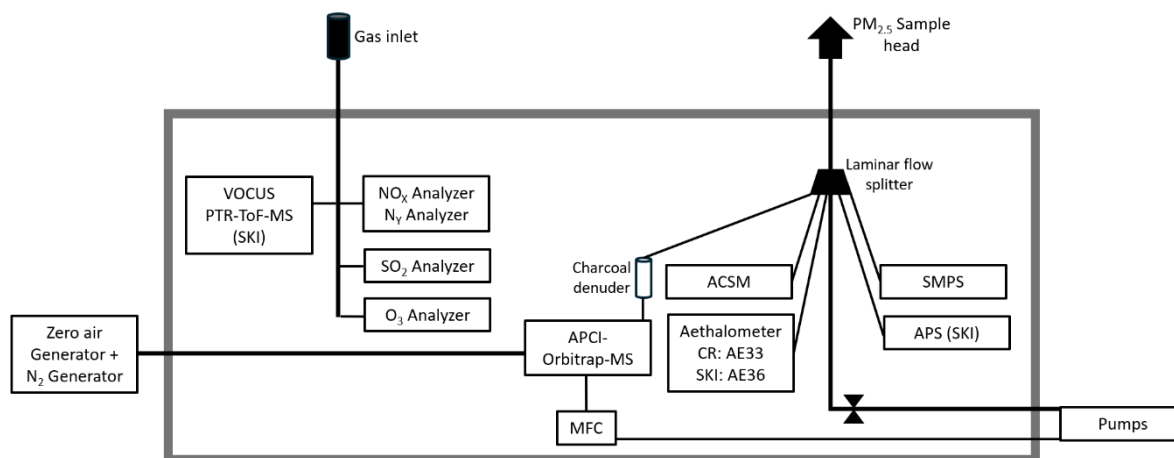
10

15

20

25

30

35

40

45



**Figure S1: Schematic of the mobile laboratory container setup (not to scale). The container (4.5 m x 1.4 m x 2.3 m, L x D x H) was equipped with an air conditioning unit to maintain temperatures between 20 °C and 24 °C. External equipment included a compressor for the zero-air and nitrogen generator (for Orbitrap calibration), pumps for the particle inlet system, SMPS, and gas monitors. Gas-phase instruments included $NO_x$, $N_Y$, $SO_2$ and $O_3$ analysers and in SKI a PTR-ToF-MS. Particle-phase measurements were conducted using a PM$_{2.5}$ inlet with regulated airflow. A laminar flow splitter distributed aerosol flow to the SMPS, ACSM, Aethalometer (CR: AE33, SKI: AE36), APS (SKI), and APCI-Orbitrap-MS. To ensure only particle-phase measurements, the aerosol flow passed through a charcoal denuder, with airflow regulated at 1.6 L min$^{-1}$ by an MFC and pump.**
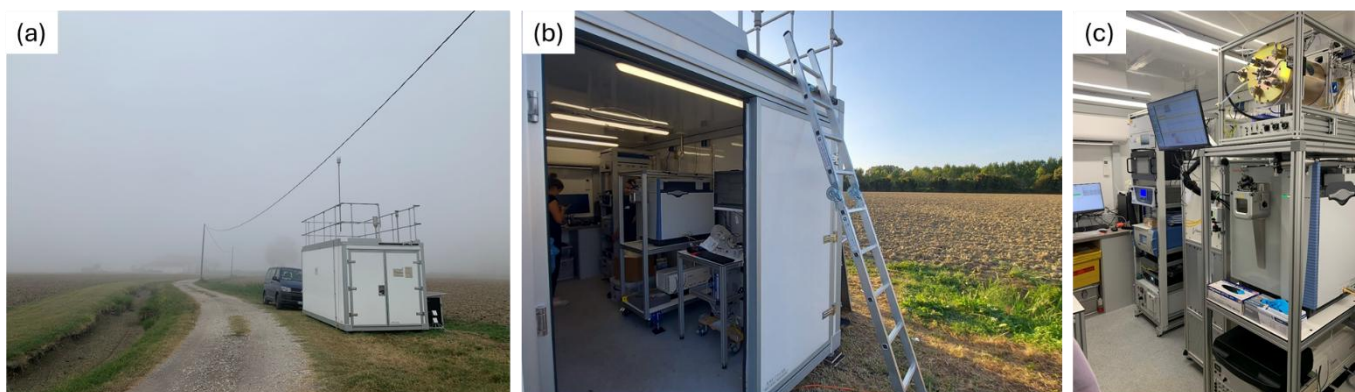


**Figure S2: Pictures of the mobile laboratory container in SKI. a) shows agricultural surrounding on a foggy day; b) closer picture showing the APCI-Orbitrap-MS and ACSM as well as agricultural field next to it; c) closeup of the APCI-Orbitrap-MS, VOCUS PTR-ToF-MS and gas monitors ($NO_X$, $N_Y$, $SO_2$, $O_3$).**
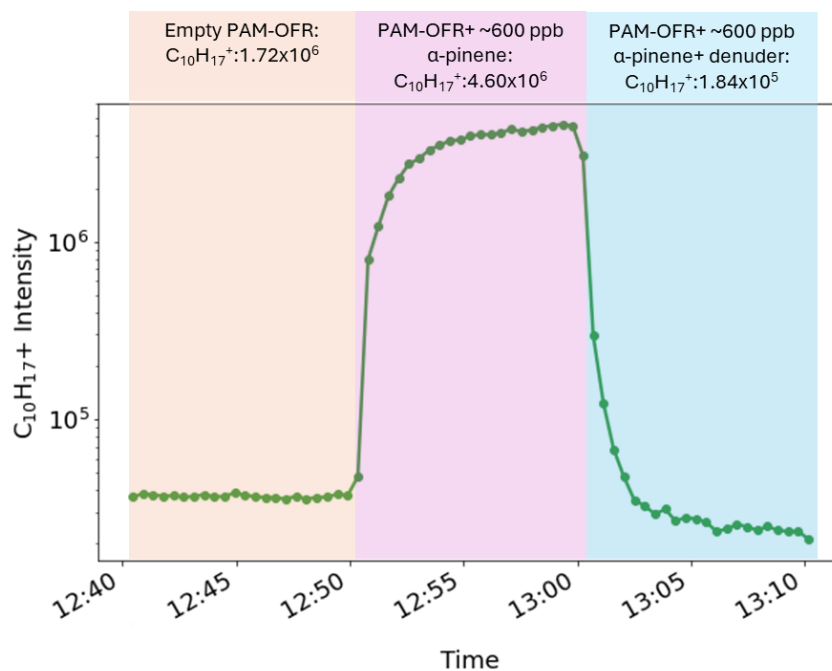
50

**Figure S3: Denuder efficiency test showing $C_{10}H_{17}^+$ intensity over time for an empty PAM-OFR (orange), ~600 ppb α-pinene in PAM-OFR (purple), and ~600 ppb α-pinene after charcoal denuder (blue).**
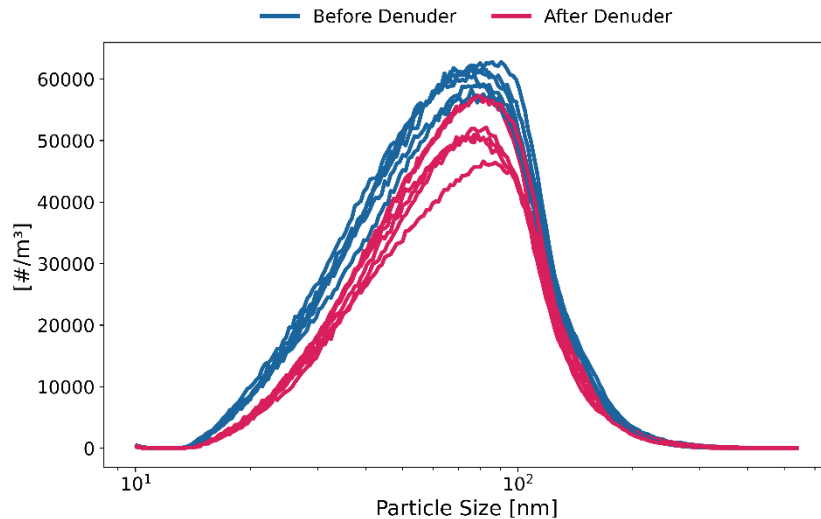
55



**Figure S4: Denuder transmission efficiencies from α-pinene PAM-OFR experiments before (blue) and after (red) the charcoal denuder for size dependent losses, shown as the particle number concentration [#/m³] over the particle size [nm] range.**
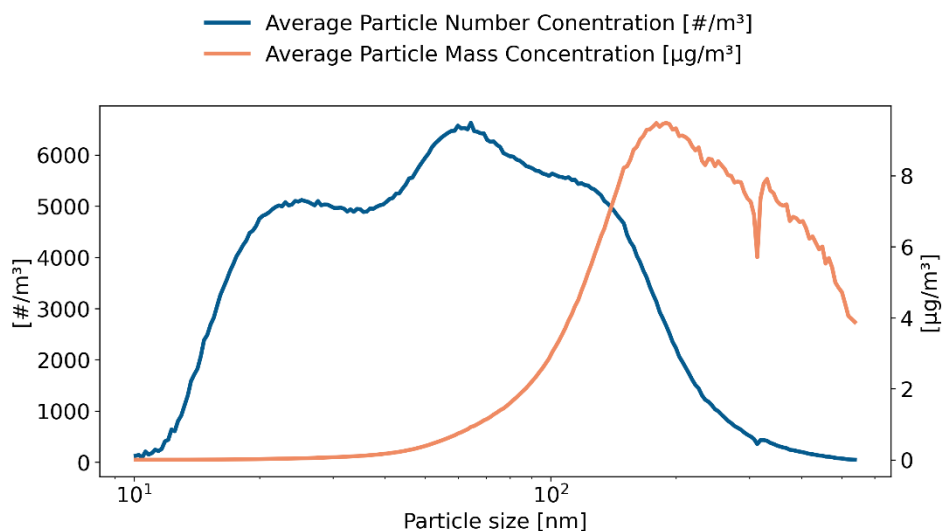
60

**Figure S5: SMPS measurements from CR between 07. July and 10. July 2023. Shown are the average particle number concentration [#/m³] in blue and Average Particle Mass Concentration [µg/m³] in orange over the measured size range [nm].**
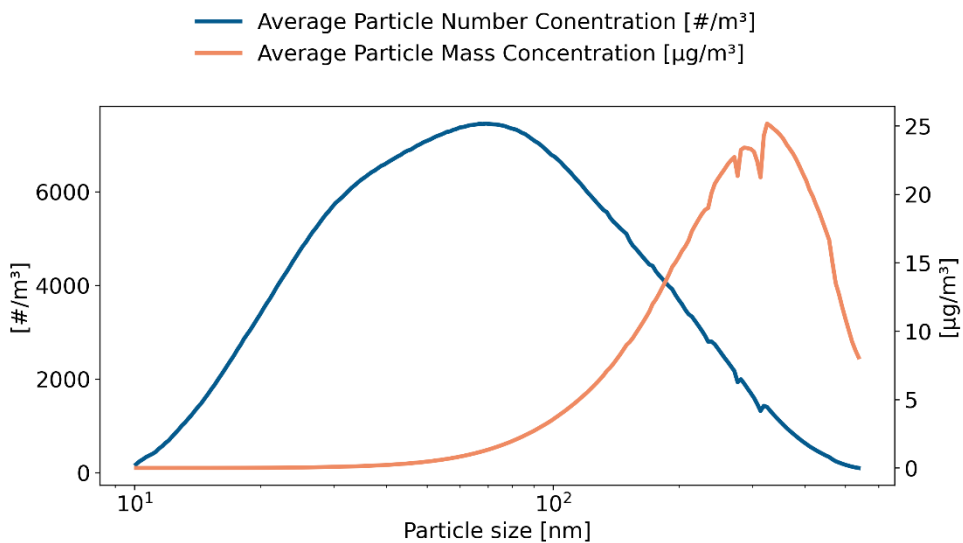
65



**Figure S6: SMPS measurements from SKI between 28 September and 04 October 2023. Shown are the average particle number concentration [#/m³] in blue and Average Particle Mass Concentration [µg/m³] in orange over the measured size range [nm].**
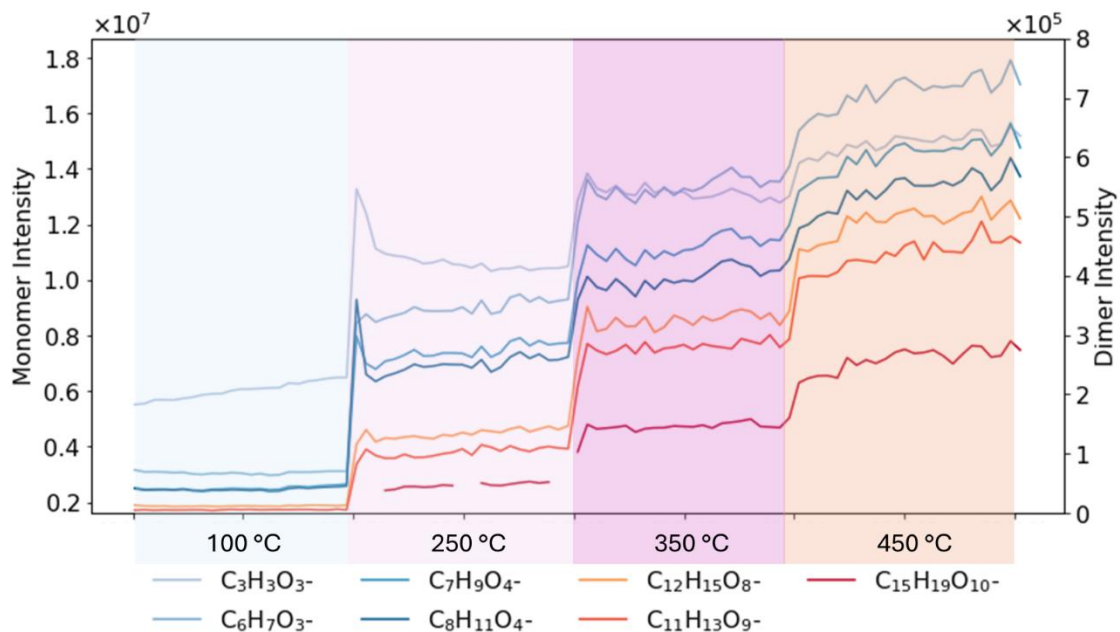
**Figure S7: Vaporizer temperature stepping experiments from 100 °C, 250 °C, 350 °C to 450 °C for monomers intensity on the left-hand y-axis in and dimers intensity on the right-hand y-axis.**
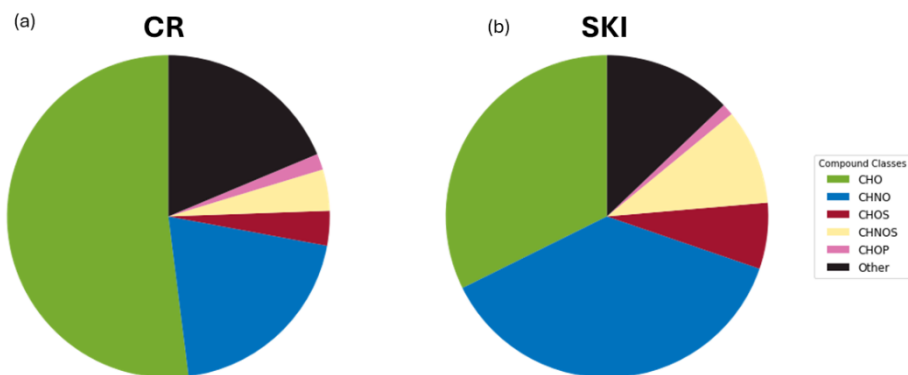


**Figure S8: Attribution of molecular formulas from negative ionization mode to different compound classes which CHO (green), CHNO (blue), CHOS (red), CHNOS (yellow), CHOP (pink) and other compounds (cyan) for (a) CR and (B) SKI.**

70

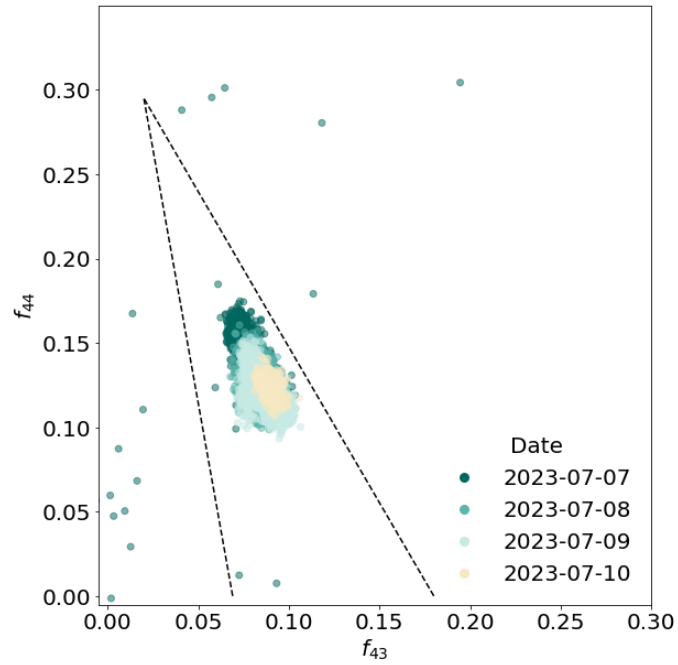**Figure S9: Triangle plot (*f*44 vs. *f*43) for CR between 07 July and 10. July 2023. The dotted lines are derived from Ng et al., (2010) indicating the area in which typical OOA lies.**
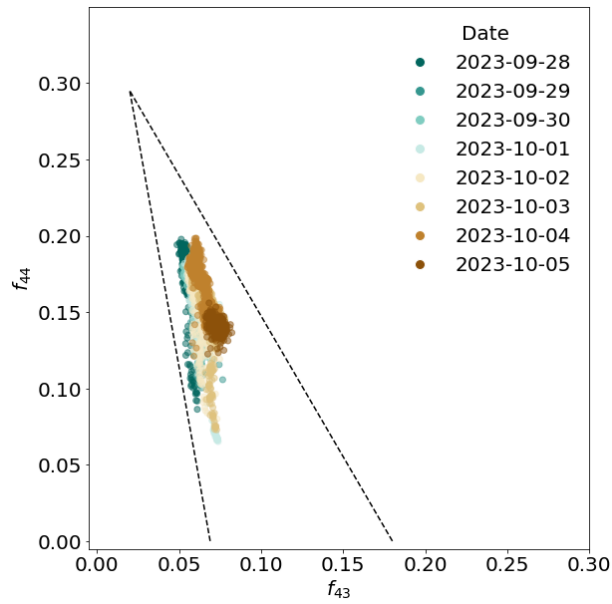


**Figure S10: Triangle plot (f44 vs. f43) for SKI between 28. September and 04. October 2023. The dotted lines are derived from Ng et al. (2010) indicating the area in which typical OOA lies.**

**Table S1: Spectral data from negative ionization mode measurements recorded in SKI on the 28 September 2023 during a BB-event. Shown are the detected peaks from *m/z* 161 to 161.09, with information about the measured peak mass, the theoretical mass, the unambiguous attributed formula, the peak intensity, the ring and double-bond (RDB) equivalents and mass deviation in delta ppm.**

| Peak Mass | Theo. mass | Displayed Formula $[M-H]^-$ | Intensity | RDB | Delta [ppm] |
|---|---|---|---|---|---|
| 161.0092 | 161.00916 | $C_5H_5O_6$ | 1.09E+04 | 3.5 | -0.06 |
| 161.0092 | | | | | |
| 161.0243 | 161.02442 | $C_9H_5O_3$ | 2.18E+04 | 7.5 | -0.19 |
| 161.0356 | 161.03565 | $C_8H_5O_2N_2$ | 2.51E+04 | 7.5 | -0.05 |
| 161.0454 | 161.04555 | $C_6H_9O_5$ | 1.83E+05 | 2.5 | -0.27 |
| 161.0608 | 161.0608 | $C_{10}H_9O_2$ | 1.51E+04 | 6.5 | -0.07 |
| 161.0721 | 161.07204 | $C_9H_9ON_2$ | 4.77E+03 | 6.5 | -0.02 |
| 161.0819 | 161.08193 | $C_7H_{13}O_4$ | 2.98E+03 | 1.5 | -0.17 |

**Table S2: Spectral data from positive ionization mode measurements recorded in SKI on the 05 October 2023 during a BB-event. Shown are the detected peaks from *m/z* 163.02 to 163.135, with information about the measured peak mass, the theoretical mass, the unambiguous attributed formula, the peak intensity, the ring and double-bond (RDB) equivalents and mass deviation in delta ppm.**

| Peak Mass | Theo. mass | Displayed Formula $[M+H]^+$ | Intensity | RDB | Delta [ppm] |
|---|---|---|---|---|---|
| 163.0236 | 163.02371 | $C_5H_7O_6$ | 1.16E+04 | 2.5 | 0.55 |
| 163.0389 | 163.03897 | $C_9H_7O_3$ | 1.43E+05 | 6.5 | 0.38 |
| 163.0502 | 163.0502 | $C_8H_7O_2N_2$ | 1.18E+05 | 6.5 | 0.26 |
| 163.0602 | 163.0601 | $C_6H_{11}O_5$ | 1.25E+05 | 1.5 | 0.31 |
| 163.0755 | 163.07536 | $C_{10}H_{11}O_2$ | 5.08E+05 | 5.5 | 0.32 |
| 163.0867 | 163.08659 | $C_9H_{11}ON_2$ | 2.18E+05 | 5.5 | 0.31 |
| 163.0948 | | | 1.28E+04 | | |
| 163.0980 | | | 7.91E+03 | | |
| 163.1061 | | | 8.56E+03 | | |
| 163.1117 | 163.11174 | $C_{11}H_{15}O$ | 5.22E+04 | 4.5 | 0.65 |
| 163.1140 | | | | | |
| 163.1230 | 163.12298 | $C_{10}H_{15}N_2$ | 3.74E+04 | 4.5 | 0.16 |
| 163.1330 | 163.13287 | $C_8H_{19}O_3$ | 6.67E+04 | -0.5 | 0.48 |

**Table S3: Attributes chemical formulas and respective intensities for each compound class in negative [M−H]⁻ and positive ionization mode [M+H]⁺.**

| Compound class | ∑Intensity | ∑Attributed formulas |
|---|---|---|
| CHO [M−H]⁻ | 9.22E+09 | 1112 |
| CHO [M+H]⁺ | 4.84E+09 | 1115 |
| CHON [M−H]⁻ | 2.22E+09 | 1287 |
| CHON [M+H]⁺ | 4.82E+09 | 1269 |
| CHOS [M−H]⁻ | 1.25E+08 | 228 |
| CHOS [M+H]⁺ | 1.41E+07 | 51 |
| CHNOS [M−H]⁻ | 8.25E+07 | 330 |
| CHNOS [M+H]⁺ | 1.60E+07 | 85 |
| CHN [M+H]⁺ | 4.34E+08 | 155 |
| Other [M−H]⁻ | 1.18E+09 | 443 |
| Other [M+H]⁺ | 7.90E+07 | 511 |

85
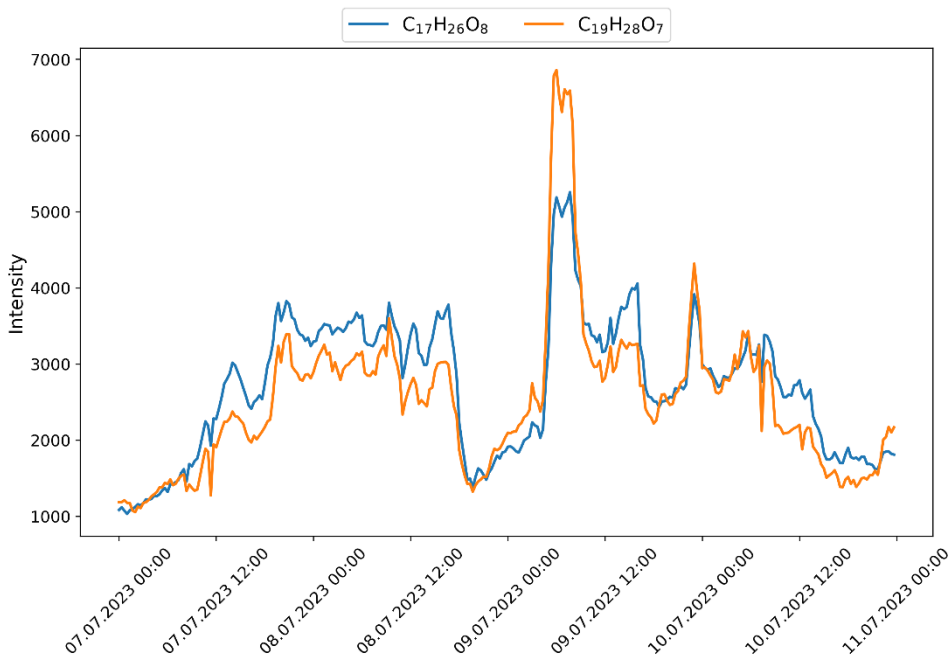


**Figure S11: 30 minutes average intensity of $C_{17}H_{26}O_8$ (blue) and $C_{19}H_{28}O_7$ (orange) during ambient measurements at CR between 07 July and 10 July 2023.**

References

Ng, N. L., Canagaratna, M. R., Zhang, Q., Jimenez, J. L., Tian, J., Ulbrich, I. M., Kroll, J. H., Docherty, K. S., Chhabra, P. S., Bahreini, R., Murphy, S. M., Seinfeld, J. H., Hildebrandt, L., Donahue, N. M., DeCarlo, P. F., Lanz, V. A., Prévôt, A. S. H., Dinar, E., Rudich, Y., and Worsnop, D. R.: Organic aerosol components observed in Northern Hemispheric datasets from Aerosol Mass Spectrometry, Atmos. Chem. Phys., 10, 4625–4641, https://doi.org/10.5194/acp-10-4625-2010, 2010.